Dual-Path Mach—Zehnder Interferometers With Unequal Geometrical Path Length for Ultrasensitive Refractive Index Sensing

Yipeng Liao, Hongcheng Wang, Shanshan Wang, Ye Liu, and Dongxiong Ling

***Abstract*—High-sensitivity fiber-optic interferometric refractive index sensors (FIRSs) have been of interest to researchers due to their potential to fabricate specific physical, chemical, and biological sensors. Fabricating interferometers working near the dispersion turning point (DTP) is an effective approach to improve the sensitivity of FIRSs. However, the group effective refractive index (RI) difference approaching 0 and the ratio of the variation of the effective RI difference to the external RI change being −1 cannot be simultaneously realized in low RI sensing, which restricts the further improvement of sensing sensitivity. Here, dual-path Mach-Zehnder interferometers (MZIs) with unequal geometrical path length are proposed for ultrasensitive RI sensing. The dual-path MZIs contain fiber path and sample path of different geometrical lengths to form the optical path difference. The dual-path MZIs can not only show a turning point where the sensing sensitivity tends to be infinite, which is similar to the previously reported DTP, but also get the constant value −1 for the RI response factor, leading to the result that the dips within an over-500-nm band width around the turning point can achieve high sensitivity reaching 10^5 nm/RIU level or higher. Ultrahigh sensitivity of -1.26×10^6 nm/RIU has been experimentally demonstrated at the RI around 1.35022. The dual-path MZIs proposed here may enlighten new ideas for developing high-sensitivity FIRSs.**

***Index Terms*—Fiber-optic sensor, Mach—Zehnder interferometer, refractive index sensor, sensitivity.**

Manuscript received July 28, 2020; revised September 25, 2020 and November 19, 2020; accepted December 22, 2020. Date of publication December 29, 2020; date of current version April 16, 2021. This work was supported by the Guangdong Basic and Applied Basic Research Foundation under Grant 2019A1515110978, in part by the China Postdoctoral Science Foundation under Grant 2020M673381, in part by the Dongguan Social Science and Technology Development Project under Grant 2019507140172, in part by the National Natural Science Foundation of China under Grants 11874111, 51771189, and 61771138, in part by the National Key Research and Development Program of China under Grant 2019YFC1511001, in part by the Guangdong Educational Commission Program under Grant 2019KZDXM016, in part by the Program of the Science and Technology Innovation Institute of Dongguan University of Technology under Grant KCYCXPT2017004, and in part by the Dongguan Core Technology Frontier Project under Grant 2019622102012. *(Corresponding authors: Hongcheng Wang; Dongxiong Ling.)*

Yipeng Liao is with the School of Electrical Engineering and Intelligentization, Dongguan University of Technology, Dongguan 523808, China, and also with the School of Science, Xi'an Jiaotong University, Xi'an 710049, China (e-mail: ypliao@dgut.edu.cn).

Hongcheng Wang, Ye Liu, and Dongxiong Ling are with the School of Electrical Engineering and Intelligentization, Dongguan University of Technology, Dongguan 523808, China (e-mail: wanghc@dgut.edu.cn; liuye@dgut.edu.cn; lingdx@dgut.edu.cn).

Shanshan Wang is with the College of Information Science and Engineering, Ocean University of China, Qingdao 266100, China (e-mail: wangshanshan@ouc.edu.cn).

Color versions of one or more of the figures in this article are available online at https://doi.org/10.1109/JLT.2020.3047943.

Digital Object Identifier 10.1109/JLT.2020.3047943

I. Introduction

HIGH-SENSITIVITY fiber-optic refractive index (RI) sensors have been of interest to researchers for a long time since RI is a fundamental optical parameter of materials or medium, and RI is not only related to numerous physical parameters such as temperature [1]–[3], deformation [4], and strain [5], but also to various chemical parameters such as humidity [6], [7] and concentration of gas or biomolecule [8]–[10], hence the construction of high-sensitivity fiber-optic RI sensor will further promote the development of specific fiber-optic physical, chemical, biological, and environmental sensors.

Currently, a variety of fiber-optic RI sensors have been proposed, mainly including fiber Bragg grating-based sensors [11], [12], microfiber resonators [13]–[15], fiber-optic surface plasmon resonance (SPR) sensors [16], and fiber-optic interferometric sensors [17]–[20]. Benefitting from the simple fabrication process, low-cost manufacturing equipment and the convenience of not requiring the assistance of a metal film, fiber-optic interferometric RI sensors (FIRSs) have become one of the most important and promising categories of fiber-optic RI sensors.

In order to fabricate high-sensitivity FIRSs, a great deal of schemes on the geometry of FIRSs have been proposed in recent years [21]–[23], such as fabricating interferometers by using fiber segments with special structure (including side-polished fiber [24], microfiber [25], thin-core fiber [26], etc.), or designing special geometries for sensor structures (including bending [27], offsetting [28], etc.), or fabricating interferometers by the combination of them [29]. Among all the schemes, fabricating interferometers working near the dispersion turning point (DTP) has been proven to be a very effective approach to significantly improve sensitivity since the sensitivity at the DTP tends to be infinite [30], and thus numerous FIRSs working near the DTP have been proposed, such as the circular microfiber-based in-line modal interferometers (MMIs) [31], [32], the microfiber couplers (MFCs) [33]–[35], the in-fiber Mach-Zehnder interferometer (MZI) formed by a microfiber-assisted U-shape cavity (MFA-USC) [36], and the optofluidic interferometer [37]. In terms of MMIs and MFCs, the DTP can be potentially achieved within a wide RI range by adjusting the microfiber diameter. However, the absolute value of the ratio of the variation of the

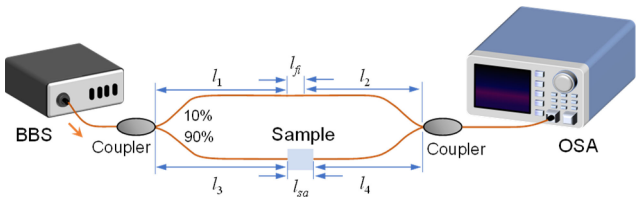

Fig. 1. Schematic diagram of the dual-path MZIs.

effective RI difference between two propagation modes to the external RI change is less than 0.5 at the DTP, which restricts the further improvement of sensing sensitivity. Furthermore, since the DTP is already near the cut-off wavelength of the higher order mode, the above-mentioned ratio will decrease rapidly as the probing wavelength moves away from the DTP to shorter wavelength, and thus the sensing sensitivity will dramatically decrease as well, finally reducing the band width to achieve high sensitivity. As for the MFA-USC and optofluidic interferometer, although the ratio of the variation of the RI difference between two paths to the external RI change has been optimized to be -1, the DTP can only be obtained when the external RI is around 1.454 [36] and 1.4 [37], respectively. When it comes to the common low RI sensing applications within 1.333–1.35, the sensing sensitivity will fall to the magnitude of 10^4 nm/RIU because of the relatively large RI difference between silica/polydimethylsiloxane (PDMS) and the sample.

To break through the limitation mentioned above, dual-path MZIs with unequal geometrical path length are proposed and optimized to perform RI sensing in this paper. The dual-path MZIs can not only show a turning point where the sensing sensitivity tends to be infinite within a wide RI range, which is similar to the previously reported MMI [32] and MFC [34], but also gets the constant value -1 for the RI response factor. As a result, the dual-path MZIs show superior sensitivity near the turning point, and the dips within an over-500-nm band width around the turning point can achieve high sensitivity reaching 10^5 nm/RIU level or higher. In particular, an ultrahigh sensitivity up to the magnitude of 10^6 nm/RIU has been experimentally demonstrated in low RI sensing for the first time. The dual-path MZIs and the strategy of unequal geometrical path length proposed here may provide a reference for developing high-sensitivity FIRSs.

II. Dual-Path Mach-Zehnder Interferometers Design and Theoretical Analysis

The schematic diagram of the dual-path MZIs is shown in Fig. 1. The dual-path MZIs consist of two arms, one of which is entirely formed by single mode fiber (SMF) and the other one contains a section of the solution to be measured as the optical path, and the geometrical length of these two arms satisfies $l_1 + l_2 = l_3 + l_4$ and $l_{fi} \neq l_{sa}$. The output intensity of the dual-path MZIs I is obtained by the superposition of intensities I_1 and I_2 of the two arms [36], [38]:

$$I = I_1 + I_2 + 2\sqrt{I_1 I_2}\cos\left(2\pi\left(n_{eff} l_{fi} - n_{sa} l_{sa}\right)/\lambda + \varphi_0\right) \tag{1}$$

where n_{eff} and n_{sa} denote the effective RI of fundamental mode and the RI of sample, respectively, and φ_0 is the initial phase of the interference. The position of the interference dips λ_D can be expressed as

$$\left(m + 1/2 - \varphi_0/(2\pi)\right)\lambda_D = n_{eff} l_{fi} - n_{sa} l_{sa} \tag{2}$$

Here, m is an integer. Let $\Delta n = n_{eff} l_{fi}/l_{sa} - n_{sa}$, and thus (2) can be rewritten as

$$\left(m + 1/2 - \varphi_0/(2\pi)\right)\lambda_D = \Delta n \cdot l_{sa} \tag{3}$$

By taking an infinitesimal variation with respect to the RI of sample from (3), we have

$$\left(m + 1/2 - \varphi_0/(2\pi)\right) d\lambda_D = l_{sa} d\left(\Delta n\right) \tag{4}$$

By solving (3) and (4), the sensing sensitivity expression of the dual-path MZIs can be deduced as

$$\begin{aligned} S = \frac{d\lambda_D}{dn_{sa}} &= \frac{\lambda_D}{\Delta n - \lambda_D \partial\left(\Delta n\right)/\partial\lambda_D} \cdot \frac{\partial\left(\Delta n\right)}{\partial n_{sa}} \\ &= \frac{\lambda_D}{n_g^{eff} l_{fi}/l_{sa} - n_g^{sa}} \cdot \frac{\partial\left(\Delta n\right)}{\partial n_{sa}} \end{aligned} \tag{5}$$

Here, $n_g{}^{eff}$ and $n_g{}^{sa}$ denote the group effective RI of fundamental mode and the group RI of sample, respectively, $\partial(\Delta n)/\partial n_{sa}$ is called as the RI response factor, and its value is constantly equal to -1. It can be seen from (5) that the sensing sensitivity of the dual-path MZIs is highly dependent on the value of geometrical parameter l_{fi}/l_{sa}. By adjusting l_{fi}/l_{sa} into a suitable value, the value of $n_g{}^{eff} l_{fi}/l_{sa} - n_g{}^{sa}$ can be tuned to 0 at a certain wavelength (i. e., the turning point), and thus the sensing sensitivity will tend to be infinite, which is similar to that at the DTP of the MMI [32] and MFC [34].

In order to study the conditions for achieving the turning point and the spectral characteristics near the turning point, the theoretical simulation was performed. Since the sensitivity characteristics are not affected by φ_0, here φ_0 was assigned as 0 to simplify the analysis. To calculate n_{eff}, SMF was considered as a circular waveguide with 8.2-μm-diameter 4% (mole fraction) GeO_2-doped silica core and pure silica cladding, and the RI of silica and GeO_2-doped silica has been given in Ref. [39]. Assuming that the dual-path MZIs with the same l_{fi} (4000 μm) but different l_{sa} (4320–4370 μm) are immersed in pure water, and the simulated normalized transmission spectra of them are shown in Fig. 2(a). It can be seen that the turning point at a shorter wavelength can be achieved in the case of a larger l_{sa}, and the free spectral range (FSR) decreases as the wavelength moves away from the turning point, which is similar to that of the MFC [34]. More specifically, the dependence of the turning point position on l_{sa}/l_{fi} ranging from 1.078 to 1.094 is shown in Fig. 2(b), which indicates that the turning point at a shorter wavelength can be obtained in the case of a larger l_{sa}/l_{fi}. Theoretically, for any value of l_{fi}, it is always possible to find the suitable value of l_{sa} to make the turning point appear in the probing band, and the turning point position can be further tuned by adjusting l_{sa}.

Then the spectral response to RI variation and the performance of the dual-path MZIs near the turning point are studied. In the

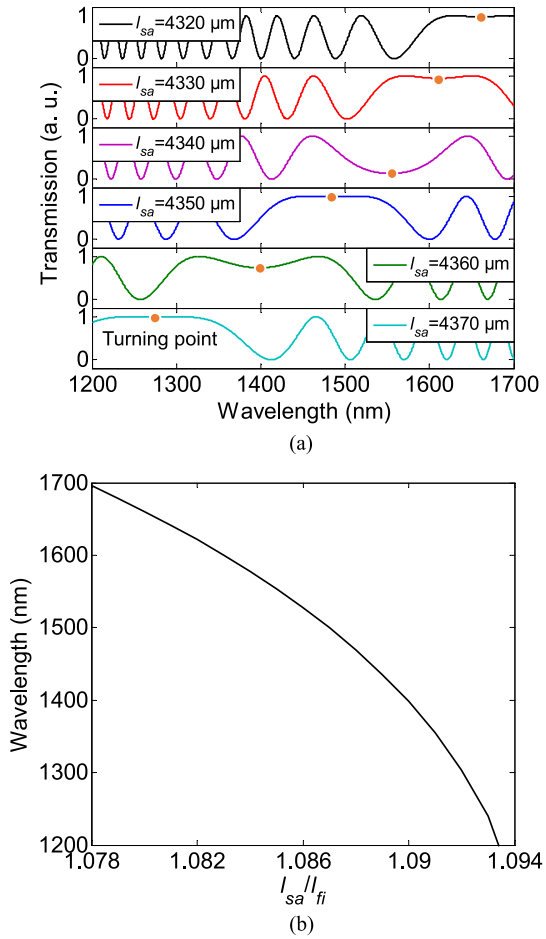

Fig. 2. (a) Simulated normalized transmission spectra of the dual-path MZIs with $l_{fi} = 4000$ μm and different l_{sa} in pure water. (b) The dependence of the turning point position on l_{sa}/l_{fi}.

theoretical model, l_{fi} and l_{sa} were firstly set as 4000 μm and 4350.4 μm, respectively, and thus the turning point is at 1482 nm when the dual-path MZI is immersed in pure water. Fig. 3(a) shows the normalized transmission spectra under different external RI change ranging from 0 to 0.00025 in steps of 0.00005. As the external RI increases, the dip at the turning point is gradually broadened and deepened. As the external RI keeps increasing, the broad dip at the turning point splits into two dips on both sides, and these two dips tend to shift backwards to the turning point. The closer the dips are to the turning point, the greater the shifts are. Meanwhile, a broad peak is formed at the turning point and will be broadened and split into two peaks on both sides. It can also be seen that the interference dips at the wavelength shorter than the turning point shift toward shorter wavelength as the external RI increases, which means that their sensitivity are negative, whereas the sensitivity of the interference dips at the wavelength longer than turning point are positive. Fig. 3(b) shows the sensitivity of the dual-path MZIs with $l_{sa}/l_{fi} = 1.0876$ versus wavelength under different external RI (1.3159–1.3219). For a dual-path MZI with specific geometrical parameters, only a series of scatters on the wavelength-sensitivity curve can be obtained, however any point on that curve can be potentially

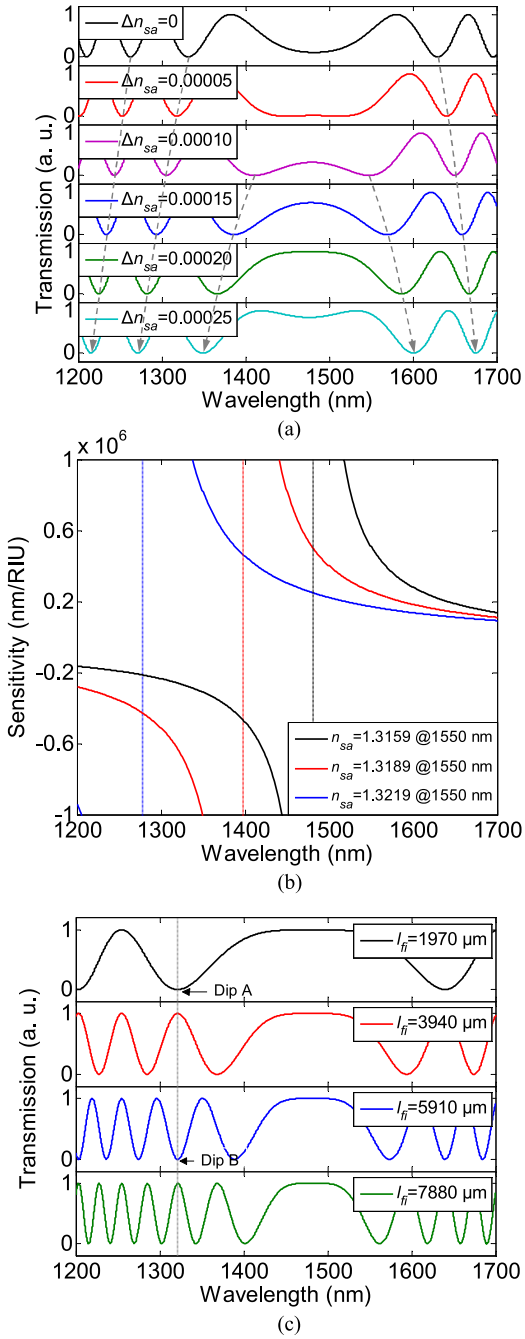

Fig. 3. (a) Simulated normalized transmission spectra of the dual-path MZI with $l_{fi} = 4000$ μm and $l_{sa} = 4350.4$ μm as the external RI increases. The initial sample is pure water. (b) RI sensing sensitivity of the dual-path MZIs with $l_{sa}/l_{fi} = 1.0876$ versus wavelength under different external RI. (c) Calculated normalized transmission spectra of the dual-path MZIs with the same value of l_{sa}/l_{fi} (1.0876) but different value of l_{fi}.

achieved by adjusting the detailed values of l_{sa} and l_{fi}. It can be noticed from Fig. 3(b) that the sensitivity at the turning point tends to be infinite, and the nearer the dips are to the turning point, the higher sensitivity can be achieved. Although the sensitivity will decrease as the probing wavelength moves away from the turning point, the dual-path MZIs still exhibits superior performance within 1200–1700 nm, where the dips can achieve high sensitivity reaching 10^5 nm/RIU level or higher, and the

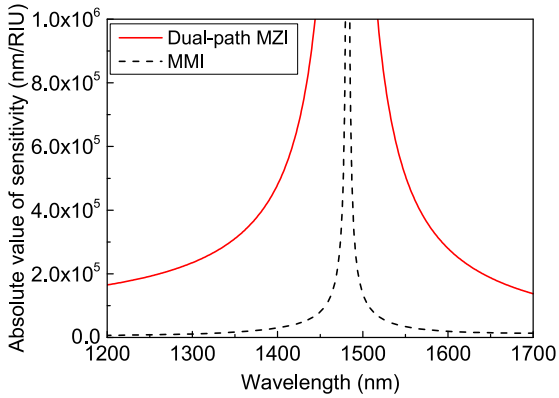

Fig. 4. Comparison for the absolute value of sensitivity of the dual-path MZI and the MMI. The DTP of MMI and the turning point of dual-path MZI are tuned into 1482 nm.

dips within an over-70-nm band width around the turning point can even achieve ultrahigh sensitivity reaching 10^6 nm/RIU level or higher. It can also be found that the turning point shifts to shorter wavelength with the increasing of external RI, which indicates that not only the turning point can be easily tuned by adjusting the external RI, but also a dual-path MZI with certain structure parameters has the capacity to achieve ultrahigh sensing sensitivity for a small range of the external RI rather than a certain external RI. Besides, in the case of a certain value of l_{sa}/l_{fi}, the dips at a same position, i. e., the same sensitivity, can be obtained under numerous sets of detailed values of l_{sa} and l_{si}, whereas these dips show different full width at half maximum (FWHM), suggesting an effective approach to improve the figure of merit (FOM). Fig. 3(c) shows the calculated normalized transmission spectra of the dual-path MZIs with $l_{sa}/l_{fi} = 1.0876$ but different value of l_{fi} (1970–7880 μm). It is clear that the dips at the same wavelength show a narrower FWHM under a larger l_{fi}, and thus the FOM can be improved by increasing the value of l_{fi} (l_{sa} should be increased in proportion as well). More exactly, the FOM of dip A in Fig. 3(c) is estimated to be -3143 RIU^{-1}, whereas the FOM of dip B rises to -9720 RIU^{-1}. On the other hand, the interference spectra of the dual-path MZIs are typically sine wave-like, and the FWHM of dips is approximately equal to half of the FSR. It is known that the dynamic range of fiber-optic interferometric sensors is generally determined by the FSR [40]. Therefore, the improvement of FOM will usually accompany by the decrease of dynamic range. For instance, although the FOM of dip B is higher than dip A, the measurement range of RI variation of dip B is only about 0.00020, which is smaller than that of dip A (0.00062). There is a tradeoff between the FOM and dynamic range of the dual-path MZIs.

Given the similarity between the sensitivity property of the dual-path MZIs and the previously reported MMI [32] and MFC [34], it is necessary to make a comparison for them. In fact, the sensitivity property of the MFC [32] is very similar to the MMI [34], and thus here we only make the comparison for the absolute value of sensitivity between the MMI and the dual-path MZI, as shown in Fig. 4, both the DTP of MMI and the turning point of dual-path MZI are adjusted into 1482 nm. It can be seen that the sensitivity of both configurations theoretically tends to be infinite at 1482 nm, however the dual-path MZI shows significantly higher sensitivity than MMI if they working at a same wavelength near the turning point/DTP. Compared with the sensitivity of the MMI, the sensitivity of the dual-path MZI also shows a much more moderate tendency to decrease as the probing wavelength shifts away from the turning point. The main reason can be explained as follows: the property of the term $n_g{}^{eff} l_{fi}/l_{sa} - n_g{}^{sa}$ of the dual-path MZI is highly similar to that of the group effective RI difference of the MMI in the whole band, which leads to the similar inverse proportional function-like change tendency of sensitivity. Nevertheless, the RI response factor of the dual-path MZI is constantly equal to -1, which is more than twice as much as the ratio of the variation of the effective RI difference between two propagation modes to the external RI change of the MMI at the DTP, and the difference between them further increases as the probing wavelength shifts toward shorter wavelength, finally resulting in the considerable difference in sensitivity. Since the dual-path MZI show high sensitivity reaching 10^5 nm/RIU level or higher within an over-500-nm band width, which is much broader than that of the MMI or MFC (about 50 nm), the dual-path MZI may maintain high sensitivity within a larger measurement range. In addition, the more moderate changing tendency of sensitivity of the dual-path MZI also indicates the better linearity of the response to RI variation.

Similarly, as we previously mentioned, there are also some FIRSs whose ratio of the variation of the RI difference between two paths to the external RI change has been optimized to be -1, such as the on-chip optofluidic interferometer [37]. However, the sensing sensitivity of the optofluidic interferometer is unchanged for a certain external RI; although the sensing sensitivity theoretically tends to be infinite when the external RI is around 1.4, it will dramatically decrease in the common low RI sensing applications since the RI difference between PDMS and sample solution increases with the decrease of RI of sample solution. In contrast, the term $n_g{}^{eff} l_{fi}/l_{sa} - n_g{}^{sa}$ of the dual-path MZIs can be optimized to approach 0 within a wide range of the external RI by adjusting the ratio of l_{sa} to l_{fi}. Here, we calculated the sensing sensitivity of the dual-path MZIs with different value of l_{sa}/l_{fi} ranging from 1.00 to 1.08 and reproduced the sensing sensitivity of the optofluidic interferometer at 1500-nm wavelength, as shown in Fig. 5. It can be seen that the ultrahigh sensing sensitivity up to the magnitude of 10^6 nm/RIU can be achieved for any external RI within 1.3159–1.4447 by adjusting l_{sa}/l_{fi}, and the sensing sensitivity of a dual-path MZI can be much higher than the optofluidic interferometer in low RI sensing applications by adjusting l_{sa}/l_{fi} into suitable values.

III. Experimental Results and Discussions

To verify the high sensing sensitivity of the dual-path MZIs, the relevant experimental works were carried out. The experimental RI sensing system, containing a broadband source (BBS) and an optical spectrum analyzer (OSA), was built as shown in Fig. 1, and the free ends of SMF were bonded on the silica glass substrate by UV glue to enhance the robustness of the

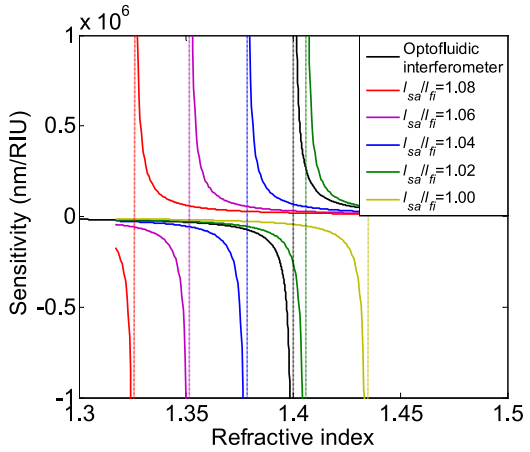

Fig. 5. Comparison for the sensing sensitivity at 1500-nm wavelength of the dual-path MZIs with different value of l_{sa}/l_{fi} and the optofluidic interferometer.

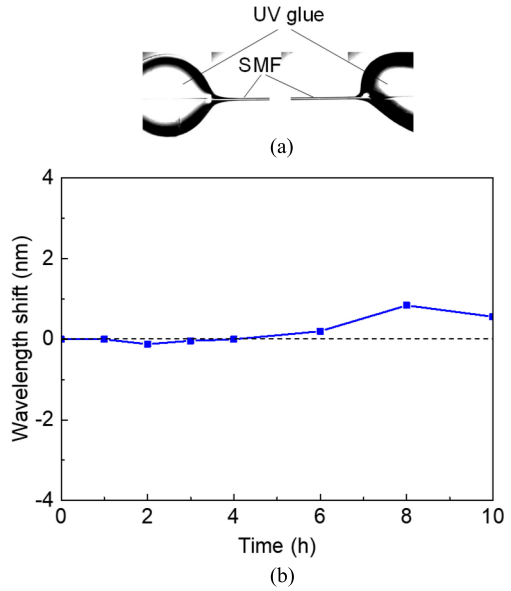

Fig. 6. (a) The photograph of the bonded free ends region of a dual-path MZI (synthesized by 4 optical micrographs). (b) The dip position fluctuation within 10 hours.

dual-path MZIs, as shown in Fig. 6(a). First of all, in order to assess the stability of the dual-path MZIs, the dip position fluctuation of a dual-path MZI was recorded at 25.0 °C for 10 hours, as shown in Fig. 6(b). It can be found that the dual-path MZI exhibits a small dip position fluctuation, which indicates the good stability to perform the subsequent RI sensing experiments. Then, a dual-path MZI with $l_{fi} = 2290.4$ μm and $l_{sa} = 2450$ μm was fabricated to perform the RI sensing experiments. In this case, the measurement range of RI variation for the dip which is nearest to the turning point is theoretically estimated to be 0.00055. To realize the tiny change of RI, the RI was changed by the use of sodium chloride solution with different mass fraction, and the real RI of the solutions n_{sa} was calculated by using the relation $n_{sa} = 1.3326 + 1.717 \times 10^{-4}M$ (M is the mass fraction in ‰), which is previously established by using an Abbe refractometer. Since the value of l_{sa}/l_{fi} is about 1.0697, the turning point is at a wavelength longer than 1700 nm in pure water environment, which is out of the probing band. Fig. 7(a) shows the transmission spectra of the dual-path MZI when taking pure water as the initial sample. With the increase of RI of solution, the interference dips shift toward shorter wavelength, which is in agreement with the theoretical simulation. Because of the strong absorption of water in the infrared band, not all of the interference dips in Fig. 7(a) show sufficiently high quality to be tracked, and the sensitivity of 4 sets of high-quality interference dips marked in Fig. 7(a) has been calculated, as shown in Fig. 7(b); the sensitivity of these 4 sets of dips reaches or exceeds the magnitude of 10^4 nm/RIU. To tune the turning point to the available probing band, according to the discussion for Fig. 3(b), the RI of solution was gradually increased. The turning point was tuned to 1627 nm, 1479 nm, and 1341 nm when the RI of solution was increased to 1.338610, 1.345478, and 1.350113, respectively. Likewise, Fig. 7(c), (e), and (g) show the spectral variation as the RI of solution changes in the above-mentioned three situations, respectively, and the high-quality dips marked in Fig. 7(c), (e), and (g) have been plotted in in Fig. 7(d), (f), and (h), respectively. It is noteworthy that a complete and clear evolution process of the turning point can be observed at 1341 nm in Fig. 7(g) and is in accordance with the theoretical simulation, and dip A in Fig. 7(g) shows an ultrahigh sensitivity of about -1.26×10^6 nm/RIU, which is the highest sensitivity among all the dips in that it is the nearest dip to the turning point among all the dips. Compared with the previously reported FIRSs working near the DTP, the sensitivity of the dual-path MZI shows a significant improvement, as shown in Fig. 8. To the best of our knowledge, the ultrahigh sensitivity demonstrated here is also the highest sensitivity which has been experimentally demonstrated in low RI sensing for FIRSs and breaks through the magnitude of 10^6 nm/RIU for the first time.

The temperature cross-sensitivity of the dual-path MZI was also evaluated. By taking an infinitesimal variation with respect to temperature from (3), we have

$$(m + 1/2 - \varphi_0/(2\pi))\, d\lambda_D = l_{sa} d(\Delta n) + \Delta n d(l_{sa}) \quad (6)$$

By solving (3) and (6), the temperature sensing sensitivity expression of the dual-path MZI can be deduced as

$$S_T = \frac{d\lambda_D}{dT} = \frac{\lambda_D}{\Delta n - \lambda_D \partial(\Delta n)/\partial\lambda_D} \cdot \left(\frac{\partial(\Delta n)}{\partial T} + \frac{\Delta n}{l_{sa}} \cdot \frac{dl_{sa}}{dT} \right) \quad (7)$$

Here, T denotes temperature. Due to the fact that l_{sa} is formed by bonding the free ends of SMF on the silica glass substrate and the thermal expansion effect of silica can be considered to be hardly affected by the polymer glue with much smaller Young's modulus [34], we have $dl_{sa} = \alpha l_{sa} dT$, here α (5.4×10^{-7}/°C) denotes the thermal expansion coefficient of silica [41]. Therefore, the temperature sensing sensitivity can be expressed as

$$S_T = \frac{\lambda_D}{\Delta n - \lambda_D \partial(\Delta n)/\partial\lambda_D} \cdot \left(\frac{l_{fi}}{l_{sa}} \frac{dn_{eff}}{dT} - \frac{dn_{sa}}{dT} + \alpha \Delta n \right) \quad (8)$$

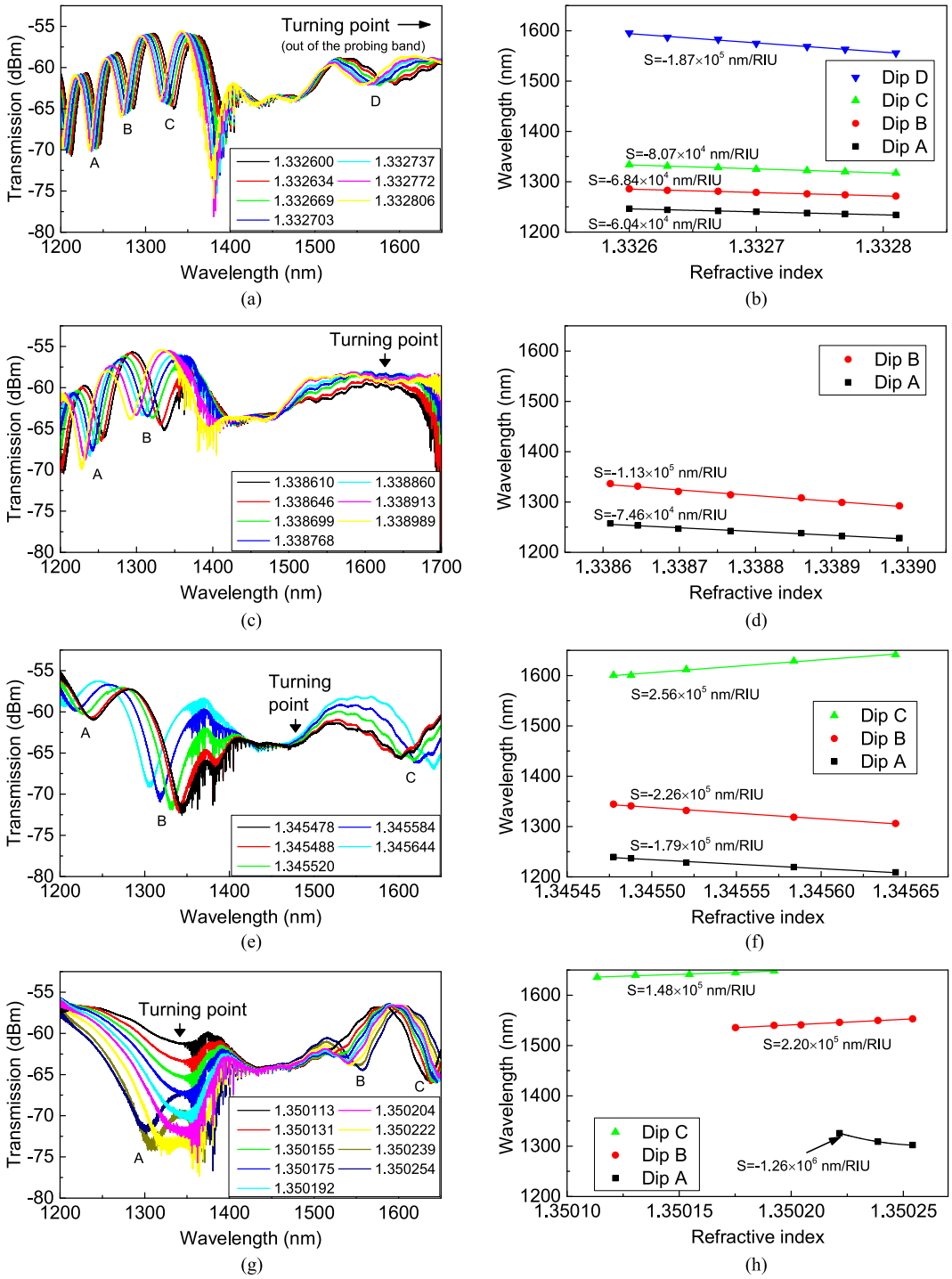

Fig. 7. Variation of the experimental transmission spectra as the RI of solution increases when the turning point is at (a) a wavelength out of the probing band, (c) 1627 nm, (e) 1479 nm, and (g) 1341 nm. (b), (d), (f), and (h) Dip wavelength shift versus the RI of solution change corresponding to (a), (c), (e), and (g), respectively.

Here, dn_{sa}/dT (-1.24×10^{-4}/°C) denote the thermo-optic coefficient (TOC) of water [41]. Compared with the expression of RI sensing sensitivity, the temperature sensing sensitivity can be also expressed as

$$S_T = -S \cdot \left(\frac{l_{fi}}{l_{sa}} \frac{dn_{eff}}{dT} - \frac{dn_{sa}}{dT} + \alpha \Delta n \right) \tag{9}$$

Since dn_{eff}/dT is approximately equal to the TOC of silica (1.18×10^{-5}/°C [41]), the temperature cross-sensitivity is approximately proportional to the RI sensing sensitivity; higher RI sensing sensitivity involves higher temperature cross-sensitivity, and the temperature cross-sensitivity is estimated to be about 172 nm/°C when the RI sensing sensitivity is -1.26×10^6 nm/RIU. Thus, the accurate temperature compensation is needed

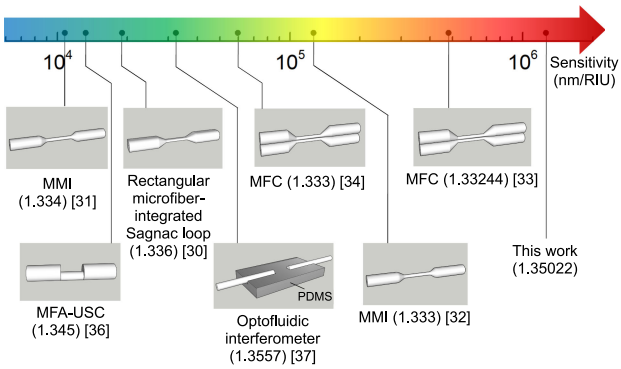

Fig. 8. The reported sensitivity of several typical FIRSs working near the turning point. The values in brackets are the external RI.

for the dual-path MZI in the actual RI sensing applications. From another point of view, the high cross-sensitivity also shows the potential of the dual-path MZI to fabricate high-sensitivity temperature sensors.

IV. Conclusion

In conclusion, this paper proposes dual-path MZIs with unequal geometrical path length for ultrasensitive RI sensing. The dual-path MZIs contain fiber path and sample path of different geometrical lengths to form the optical path difference. The sensitivity of the dual-path MZIs is highly dependent on the length ratio of fiber path and sample path. By adjusting the length ratio, the dual-path MZIs can show a turning point where the sensing sensitivity tends to be infinite within the wavelength range of 1200–1700 nm for any external RI within 1.3159–1.4447, which is similar to the previously reported MMI [32] and MFC [34]. Since the RI response factors of the dual-path MZIs are equal to -1, the dual-path MZIs show superior sensitivity near the turning point, and the dips within an over-500-nm band width around the turning point can achieve high sensitivity reaching 10^5 nm/RIU level or higher. Experimentally, an ultrahigh sensitivity up to -1.26×10^6 nm/RIU has been demonstrated, and it is the highest sensitivity in low RI sensing for FIRSs and reaches the magnitude of 10^6 nm/RIU for the first time. The dual-path MZIs proposed in this paper will enlighten new ideas for developing high-sensitivity FIRSs, and they may be further combined with polymers, magnetic fluids, etc. to develop high-performance temperature and magnetic field sensors. Finally, it should be noted that due to the use of couplers, the structure of the dual-path MZIs is rather loose, especially compared with MFC [34] or the on-chip sensor [37], therefore, fabricating dual-path MZIs without couplers by using the advanced manufacturing technology such as femtosecond laser processing technology or developing on-chip structure may be a good strategy to develop high-sensitivity and compact FIRSs in the future.

References

[1] Y. Huang *et al.*, "Nonradiation cellular thermometry based on interfacial thermally induced phase transformation in polymer coating of optical microfiber," *ACS Appl. Mater. Interfaces*, vol. 9, no. 10, pp. 9024–9028, 2017.

[2] H. Yang, J. Wang, Y. Liao, S. Wang, and X. Wang, "Dual-point seawater temperature simultaneous sensing based on microfiber double knot resonators," *IEEE Sens. J.*, vol. 17, no. 8, pp. 2398–2403, Apr. 2017.

[3] Y. Jiang, Z. Fang, Y. Du, E. Lewis, G. Farrell, and P. Wang, "Highly sensitive temperature sensor using packaged optical microfiber coupler filled with liquids," *Opt. Express*, vol. 26, no. 1, pp. 356–366, 2018.

[4] J. Villatoro, A. V. Newkirk, E. Antonio-Lopez, J. Zubia, A. Schülzgen, and R. Amezcua-Correa, "Ultrasensitive vector bending sensor based on multicore optical fiber," *Opt. Lett.*, vol. 41, no. 4, pp. 832–835, 2016.

[5] J. Li, J. Chen, S. Yan, Y. Ruan, F. Xu, and Y. Lu, "Versatile hybrid plasmonic microfiber knot resonator," *Opt. Lett.*, vol. 42, no. 17, pp. 3395–3398, 2017.

[6] Y. Huang *et al.*, "High-performance fibre-optic humidity sensor based on a side-polished fibre wavelength selectively coupled with graphene oxide film," *Sens. Actuator B-Chem.*, vol. 255, pp. 57–69, 2018.

[7] B. C. Yao *et al.*, "Graphene enhanced evanescent field in microfiber multimode interferometer for highly sensitive gas sensing," *Opt. Express*, vol. 22, no. 23, pp. 28154–28162, 2014.

[8] K. Kim, P. Lu, J. T. Culp, and P. R. Ohodnicki, "Metal−organic framework thin film coated optical fiber sensors: A novel waveguide-based chemical sensing platform," *ACS Sens*, vol. 3, no. 2, pp. 386–394, 2018.

[9] L. Sun *et al.*, "High sensitivity ammonia gas sensor based on a silica-gel-coated microfiber coupler," *J. Lightw. Technol.*, vol. 35, no. 14, pp. 2864–2870, Jul. 2017.

[10] B. Song, H. Zhang, B. Liu, W. Lin, and J. Wu, "Label-free in-situ real-time DNA hybridization kinetics detection employing microfiber-assisted Mach—Zehnder interferometer," *Biosens. Bioelectron.*, vol. 81, pp. 151–158, 2016.

[11] Y. Liu, C. Meng, A. P. Zhang, Y. Xiao, H. Yu, and L. Tong, "Compact microfiber Bragg gratings with high-index contrast," *Opt. Lett.*, vol. 36, no. 16, pp. 3115–3117, 2011.

[12] X. Fang, C. R. Liao, and D. N. Wang, "Femtosecond laser fabricated fiber Bragg grating in microfiber for refractive index sensing," *Opt. Lett.*, vol. 35, no. 7, pp. 1007–1009, 2010.

[13] X. Guo and L. Tong, "Supported microfiber loops for optical sensing," *Opt. Express*, vol. 16, no. 19, pp. 14429–14434, 2008.

[14] Y. Liao, J. Wang, H. Yang, X. Wang, and S. Wang, "Salinity sensing based on microfiber knot resonator," *Sens. Actuator A-Phys.*, vol. 233, pp. 22–25, 2015.

[15] F. Xu, P. Horak, and G. Brambilla, "Optical microfiber coil resonator refractometric sensor," *Opt. Express*, vol. 15, no. 12, pp. 7888–7893, 2007.

[16] C. Caucheteur, T. Guo, F. Liu, B. Guan, and J. Albert, "Ultrasensitive plasmonic sensing in air using optical fibre spectral combs," *Nat. Commun.*, vol. 7, 2016, Art. no. 13371.

[17] M. Janik, M. Koba, K. Król, P. Mikulic, W. J. Bock, and M. Smietana, "Combined long-period fiber grating and microcavity in-line Mach—Zehnder interferometer for refractive index measurements with limited cross-sensitivity," *Sensors*, vol. 20, no. 8, 2020, Art. no. 2431.

[18] J. Sadeghi, A. H. B. Ghasemiab, and H. Latifi, "A label-free infrared opto-fluidic method for real-time determination of flow rate and concentration with temperature cross-sensitivity compensation," *Lab Chip*, vol. 16, pp. 3957–3968, 2016.

[19] X. Li, L. V. Nguyen, Y. Zhao, H. Ebendorff-Heidepriem, and S. C. Warren-Smith, "High-sensitivity Sagnac-interferometer biosensor based on exposed core microstructured optical fiber," *Sens. Actuator B-Chem.*, vol. 269, pp. 103–109, 2018.

[20] Y. Liu and S. Qu, "Optical fiber Fabry—Perot interferometer cavity fabricated by femtosecond laser-induced water breakdown for refractive index sensing," *Appl. Opt.*, vol. 53, no. 3, pp. 469–474, 2014.

[21] M. R. Islam, M. M. Ali, M. Lai, K. S. Lim, and H. Ahmad, "Chronology of Fabry—Perot interferometer fiber-optic sensors and their applications: A review," *Sensors*, vol. 14, no. 4, pp. 7451–7488, 2014.

[22] A. Urrutia, I. Del Villar, P. Zubiate, and C. R. Zamarreño, "A comprehensive review of optical fiber refractometers: Toward a standard comparative criterion," *Laser Photon. Rev*, vol. 13, 2019, Art. no. 1900094.

[23] J. Chen, D. Li, and F. Xu, "Optical microfiber sensors: Sensing mechanisms, and recent advances," *J. Lightw. Technol.*, vol. 37, no. 11, pp. 2577–2589, Jun. 2019.

[24] R. Chu *et al.*, "All-optical graphene-oxide humidity sensor based on a side-polished symmetrical twin-core fiber michelson interferometer," *Sens. Actuator B-Chem.*, vol. 284, pp. 623–627, 2019.

[25] Y. Bai, Y. Miao, H. Zhang, and J. Yao, "Simultaneous measurement of temperature and relative humidity based on a microfiber sagnac loop and MoS_2," *J. Lightw. Technol.*, vol. 38, no. 4, pp. 840–845, Feb. 2020.

[26] T. Liu, J. Wang, Y. Liao, L. Yang, and S. Wang, "Splicing point tapered fiber Mach—Zehnder interferometer for simultaneous measurement of temperature and salinity in seawater," *Opt. Express*, vol. 27, no. 17, pp. 23905–23918, 2019.
[27] X. Zhang and W. Peng, "Bent fiber interferometer," *J. Lightw. Technol.*, vol. 33, no. 15, pp. 3351–3356, Aug. 2015.
[28] J. Li *et al.*, "Ultrasensitive refractive index sensor based on enhanced vernier effect through cascaded fiber core-offset pairs," *Opt. Express*, vol. 28, no. 3, pp. 4145–4155, 2020.
[29] T. Liu, J. Wang, Y. Liao, X. Wang, and S. Wang, "All-fiber Mach—Zehnder interferometer for tunable two quasi-continuous points' temperature sensing in seawater," *Opt. Express*, vol. 26, no. 9, pp. 12277–12290, 2018.
[30] J. Li *et al.*, "Ultrasensitive refractive-index sensors based on rectangular silica microfibers," *Opt. Lett.*, vol. 36, no. 18, pp. 3593–3595, 2011.
[31] H. Luo *et al.*, "Refractive index sensitivity characteristics near the dispersion turning point of the multimode microfiber-based Mach—Zehnder interferometer," *Opt. Lett.*, vol. 40, no. 21, pp. 5042–5045, 2015.
[32] J. Wang, Y. Liao, S. Wang, and X. Wang, "Ultrasensitive optical sensing in aqueous solution based on microfiber modal interferometer," *Opt. Express*, vol. 26, no. 19, pp. 24843–24853, 2018.
[33] W. Talataisong, R. Ismaeel, T. Lee, M. Beresna, and G. Brambilla. "Optical nanofiber coupler sensors operating in the cut-off wavelength region," *IEEE Sens. J.*, vol. 18, no. 7, pp. 2782–2787, Apr. 2018.
[34] K. Li, N. M. Y. Zhang, N. Zhang, T. Zhang, G. Liu, and L. Wei, "Spectral characteristics and ultrahigh sensitivities near the dispersion turning point of optical microfiber couplers," *J. Lightw. Technol.*, vol. 36, no. 12, pp. 2409–2415, Jun. 2018.
[35] K. Li, T. Zhang, G. Liu, N. Zhang, M. Zhang, and L. Wei, "Ultrasensitive optical microfiber coupler based sensors operating near the turning point of effective group index difference," *Appl. Phys. Lett.*, vol. 109, 2016, Art. no. 101101.
[36] S. Gao *et al.*, "Ultrasensitive refractive index sensor based on microfiber-assisted U-shape cavity," *IEEE Photon. Technol. Lett.*, vol. 25, no. 18, pp. 1815–1818, Sep. 2013.
[37] L. P. Sun *et al.*, "Ultrasensitive optofluidic interferometer for online monitoring of photocatalytic reactions," *J. Lightw. Technol.*, vol. 37, no. 21, pp. 5435–5441, Nov. 2019.
[38] Y. Li, X. Wang, and X. Bao, "Sensitive acoustic vibration sensor using single-mode fiber tapers," *Appl. Opt.*, vol. 50, no. 13, pp. 1873–1878, 2011.
[39] J. W. Fleming, "Dispersion in GeO_2–SiO_2 glasses," *Appl. Opt.*, vol. 23, no. 24, pp. 4486–4493, 1984.
[40] J. Wang, X. Li, J. Fu, and K. Li, "High-sensitivity, large dynamic range refractive index measurement using an optical microfiber coupler," *Sensors*, vol. 19, no. 23, 2019, Art. no. 5078.
[41] R. Martínez-Manuel, D. A. May-Arrioja, J. Acevedo-Mijangos, R. F. Domínguez-Cruz, D. López-Cortés, and M. Torres-Cisneros, "Ultra-high-sensitivity temperature sensor using a fiber loop mirror based on a water-filled asymmetric two-hole fiber," *IEEE Sensors J.*, vol. 20, no. 11, pp. 5953–5961, Jun. 2020.

Yipeng Liao received the B.S. degree in optical information science and technology in 2014 and the Ph.D. degree in marine detection technology in 2019 from the Ocean University of China, Qingdao, China. He is currently a Joint Postdoctoral Researcher with the Dongguan University of Technology, Dongguan, China, and Xi'an Jiaotong University, Xi'an, China. His research interests include high-performance fiber-optic sensor design and its applications.

Hongcheng Wang received the Ph.D. degree in optics from Sun Yat-sen University, Guangzhou, China, in 2007. He is currently a Professor with the School of Electrical Engineering And Intelligentization, Dongguan University of Technology, Dongguan, China. His research interests include linear and nonlinear optical beam interactions, synthetic optical materials, optical solitons, and micro- or nanofiber-based optical devices.

Shanshan Wang received the Ph.D. degree in optical engineering from Zhejiang University, Hangzhou, China, in 2010. She is currently an Associate Professor with the Department of Physics, Ocean University of China, Qingdao, China. Her research interests include nanophotonics and optical fiber sensing.

Ye Liu received the B.S. degree in optical information science and technology from Beijing Jiaotong University, Beijing, China, in 2005 and the Ph.D. degree in optics from the Institute of Physics, Chinese Academy of Sciences, Beijing, China, in 2010. She is currently a Professor with the Dongguan University of Technology, Dongguan, China, and the Director of the Department of Physics And Optoelectronic Engineering. Her research interests include micro- or nanosensors, fiber sensors, and laser spectroscopy technology.

Dongxiong Ling received the B.S. degree in laser physics from the Huazhong University of Science and Technology of China, Wuhan, China, in 1985, the M.S. degree in laser technology from the Electronics University of Science and Technology of China, Chengdu, China, in 1988, and the Ph.D. degree in materials science from the Kunming University of Science and Technology of China, Kunming, China, in 2004. He is currently a Professor with the School of Electrical engineering and Intelligentization, Dongguan University of Technology, Dongguan, China. His research interests include optical sensing, optoelectronics, and laser technology.